Hindawi
Geofluids
Volume 2021, Article ID 5598069, 17 pages
https://doi.org/10.1155/2021/5598069

Research Article

Coupling Relationship between Multistage Fluid Activity and Reservoir Abnormally High-Porosity Zones in the Songtao–Baodao Region, Qiongdongnan Basin

Xu Chen,[1,2,3] **Yao Wang**,[4] **and Ao Su**[2,3]

[1]*Cooperative Innovation Center of Unconventional Oil and Gas (Ministry of Education & Hubei Province), Yangtze University, Wuhan 430100, China*
[2]*Key Laboratory of Exploration Technologies for Oil and Gas Resources, Ministry of Education, Yangtze University, Wuhan 430100, China*
[3]*School of Geoscience, Yangtze University, Wuhan 430100, China*
[4]*School of Advanced Manufacturing Engineering, Chongqing University of Posts and Telecommunications, Chongqing 400065, China*

Correspondence should be addressed to Ao Su; suao446@163.com

Received 20 January 2021; Revised 6 April 2021; Accepted 26 April 2021; Published 17 May 2021

Academic Editor: Rongxi Li

An abnormally high-porosity zone (AHPZ) is beneficial for petroleum exploration, especially for the deep tight reservoirs in a petroliferous basin. Because of lacking effective research methods, it is hard to analyze the formation process of AHPZs in different geological periods. From the perspective of the diagenetic fluid type and activity history, geochemical characteristics and fluid inclusions of diagenetic minerals were utilized to reconstruct the diagenetic fluid type and dynamic evolution. The ultimate goal is to study the genetic process of AHPZs in the Songtao–Baodao region of the Qiongdongnan basin, South China Sea. It was found that there are three sections of AHPZs at different burial depths, which are generally favorable for high-quality reservoirs. Moreover, it can be concluded that the AHPZs are closely related to multiple actions of various diagenetic fluids. The meteoric waters, organic acid, and thermal fluids facilitated the enlargement of porosity by dissolving minerals to form secondary pore spaces. The hydrocarbon fluids have positive effects on the preservation of pores by preventing cement from filling the pore space.

1. Introduction

The development of abnormally high-porosity zones (AHPZs) in sedimentary basins has always been an important topic, which is of great significance for high-quality reservoir predictions and commercial oil-gas exploration [1]. Main mechanisms for the formation of AHPZs commonly include sedimentation, grain coat, hydrocarbon filling, overpressure, and dissolution [2, 3]. Sedimentation can control original physical properties of the sandstone reservoir. In other words, the reservoir physical properties are closely related to the sedimentary environment. In addition, sedimentation also affects diagenetic alternation. For example, sandbody that contains high content of rigid particles, few argillaceous impurities, and coarser grain generally has a strong resistance to compaction during burial, thereby preserving more pores at the same burial depth. The cementation is generally weak in the middle of thick sandbody, and the pore is relatively well preserved [4]. Grain coat grows outward from the surface of skeleton grains. It can hinder the development of quartz cements and enable the pores to be effectively preserved in the middle-deep reservoirs [5]. During reservoir diagenesis, early hydrocarbon filling can hinder the flow of pore waters and cause ion supply and flow barriers, which would inhibit or even stop the precipitation of authigenic cements and thus effectively preserve the reservoir pore [6]. An important function of fluid overpressure is to reduce the effective stress on the formation. Effective stress is an important factor controlling the compaction of

clastic rock, so fluid overpressure can inhibit the compaction, which is beneficial to the preservation of reservoir space [7, 8].

The contribution of dissolution to an abnormally high-porosity zone lies in the dissolution of unstable minerals and the formation of additional secondary pores [9]. The geological factors controlling the AHPZ development are closely associated with the types and activities of diagenetic fluids [10]. The physical and chemical properties (such as acid, alkali, temperature, pressure, and components) of the fluid affect the reservoir diagenesis and control fluid-rock interaction. The fluids affecting the reservoir can be divided into organic and carbonic acid fluids [11, 12], meteoric water [13, 14], thermal fluids [15], H_2S generated by thermochemical sulfate reduction (TSR) [16], H^+ released by clay mineral conversion [17], acid generated by biodegradable hydrocarbons [18], and alkaline fluids [19]. Most AHPZs that developed in sedimentary basins are the result of the comprehensive superposition of different factors. Therefore, the analysis of the diagenetic pore fluid type and the evolution of the AHPZs in different geological periods are difficult to analyze and often ignored by scholars. Therefore, the key to better understanding AHPZ genesis is to clarify the fluid types and their large-scale activity in the geological periods. Because of the difference in source rock types, transport systems, thermal-burial-tectonic history, and hydrocarbon migration, the diagenetic fluid types and effective activity periods are different, which have a large influence on the lateral and vertical distributions of AHPZs.

The Qiongdongnan basin is one of the most important oil-bearing basins in the South China Sea. At present, there are few wells in the eastern part of the basin, and the degree of oil-gas exploration is low. There are few reports on the formation of AHPZ in this area. In terms of sedimentary facies and environment, previous authors have analyzed the good physical properties of a deep braided river reservoir [20, 21]. The high content of quartz in sandstone has a stronger compressive ability during compaction of the overburden strata; hence, the reservoir retains more pores [22]. In addition, compaction and cementation reduce reservoir porosity, and dissolution of silicate minerals such as feldspar and rock debris plays a constructive role in reservoirs with abnormally high porosity [22, 23]. The previous studies have not systematically analyzed the causes and distribution of AHPZ, which restricts the understanding of high-quality reservoir exploration. Based on the analysis of diagenetic fluid type and activity history, this study discusses the multistage dynamic evolution process of the abnormally high-porosity zone in the study area, which is of valuable and practical significance for high-quality reservoir exploration.

2. Geological Setting

The Qiongdongnan basin is located in the northwest continental margin of the South China Sea, covering an area of about $6.3 \times 10^4\ km^2$. It is an extensional basin on the continental margin. Generally, this basin experienced two tectonic evolutionary stages: (1) the rift stage, from the Late Oligocene to Paleocene; (2) the depression stage, from the Miocene to Present [24]. It suffered from four successive tectonic episodes, including the Shenhu, Zhujiang, Nanhai, and Dongsha Movements [25]. The basin has normal faults in the lower part (Paleogene), which is overlain by Neogene sedimentary rocks within the depression. The boundary marked by the T60 forms an unconformity (Figure 1). The Cenozoic stratigraphy consists of Eocene (E_2), Lower Oligocene Yacheng Formation (E_3y), Upper Oligocene Lingshui Formation (E_3l), Lower Miocene Sanya Formation (N_1s), Middle Miocene Meishan Formation (N_1m), Upper Miocene Huangliu Formation (N_1h), Pliocene Yinggehai Formation (N_2y), and Quaternary Ledong Formation (Q_l), from bottom to top (Figure 2).

The study area is located in the Songtao–Baodao region in the eastern Qiongdongnan basin. This area is bounded by the Shenhu uplift and is adjacent to the Zhujiangkou basin. The burial histories of the eastern and western parts of the basin are different [25]. The western part experienced a slow burial at an early stage, followed a rapid burial in the late stage. In contrast, the eastern part went through a generally long-term, continuous burial. The geothermal gradient in the eastern basin (including the Songtao–Baodao region) is generally high, approximately 3.8~4°C/100 m. The current formation is hydrostatically pressured or weakly overpressured. The degree of exploration in the Songtao–Baodao region is low with few discovered petroleum structures (Figure 1). The main source rocks are coal measures in the Yacheng Formation and marine mudstones in the Lingshui Formation. The rock type of the reservoir sandstone is mainly feldspathic quartz sandstone, with a low content of rock debris (5.7%) and a medium to high compositional maturity. The textural maturity of the reservoir sandstone is relatively high because of its distance from the source area. The interstitial materials in the rock particles are mainly cement and argillaceous materials. The authigenic minerals are mainly carbonate cement, secondary quartz, and clay minerals [26].

3. Samples and Methods

Forty sandstone samples collected from the Songtao–Baodao region were used for petrologic characterization, diagenesis observation, and carbon isotope analysis, which were applied to the investigation of diagenesis observation, porosity type, and CO_2 origin. The well logs, strata division, stratigraphic age, vitrinite reflectance and measured temperature, formation tests, lithology, sandstone compositions, source rock data, and porosity-permeability data were collected from the CNOOC Research Institute. Eighteen sandstone samples from the three sections at unusually large depth in the Songtao–Baodao regions were collected; fluid inclusion analyses, including inclusion petrography, microscopic fluorescence spectrum analysis, and microthermometric measurements, were carried out. Fluid inclusion homogenization temperature (Th) combined with burial history was used to determine hydrocarbon filling time. In order to perform the diagenesis analysis, twenty samples were observed using a polarized optical microscope and an S4800 scanning electron microscope (SEM).

Carbon and oxygen isotopes of the carbonate cements were measured using a Delta Plus XL (Thermo/Finnigan) gas chromatography-carbon isotope mass spectrometer. CO_2 was collected from the selected sandstone samples using the acid solution method. The fused silica capillary column (PoraPLOT

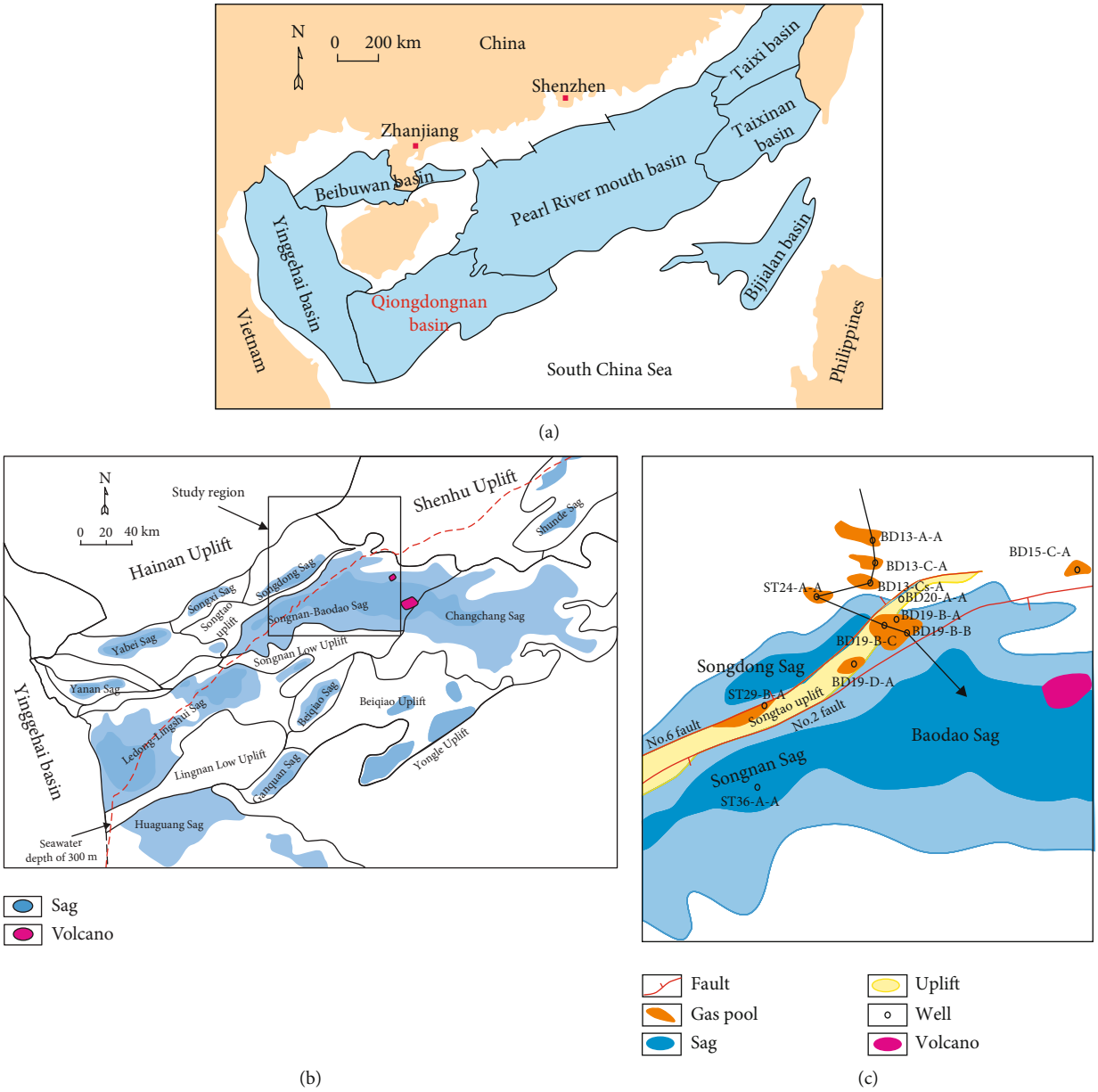

Figure 1: Continued.

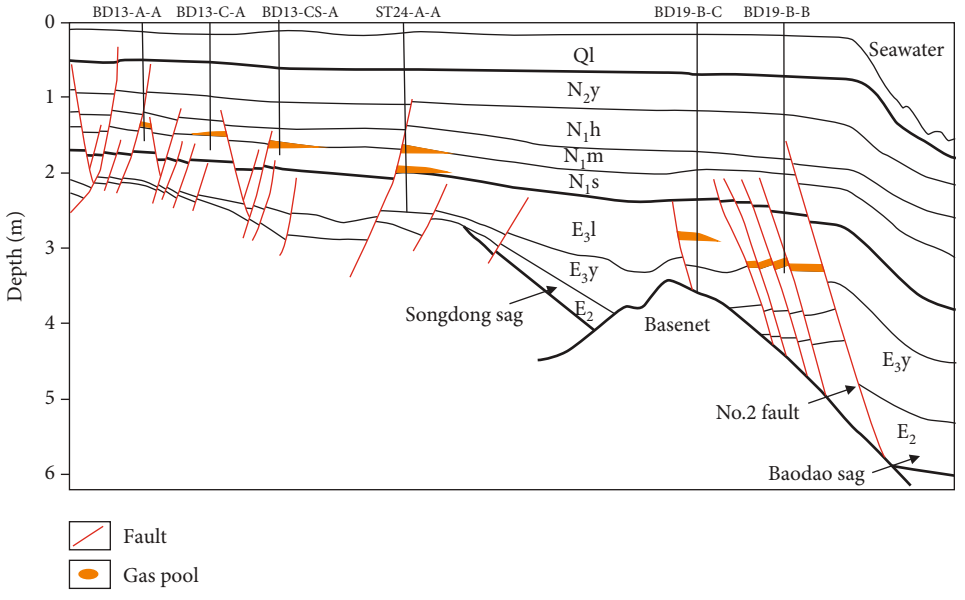

(d)

Figure 1: The location and geology of the Qiongdongnan basin: (a) map showing the Qiongdongnan basin in the South China Sea, (b) tectonic setting of the Qiongdongnan basin and location of the study area, (c) the Songtao–Baodao region and the profile location, and (d) the geological profile of the study area.

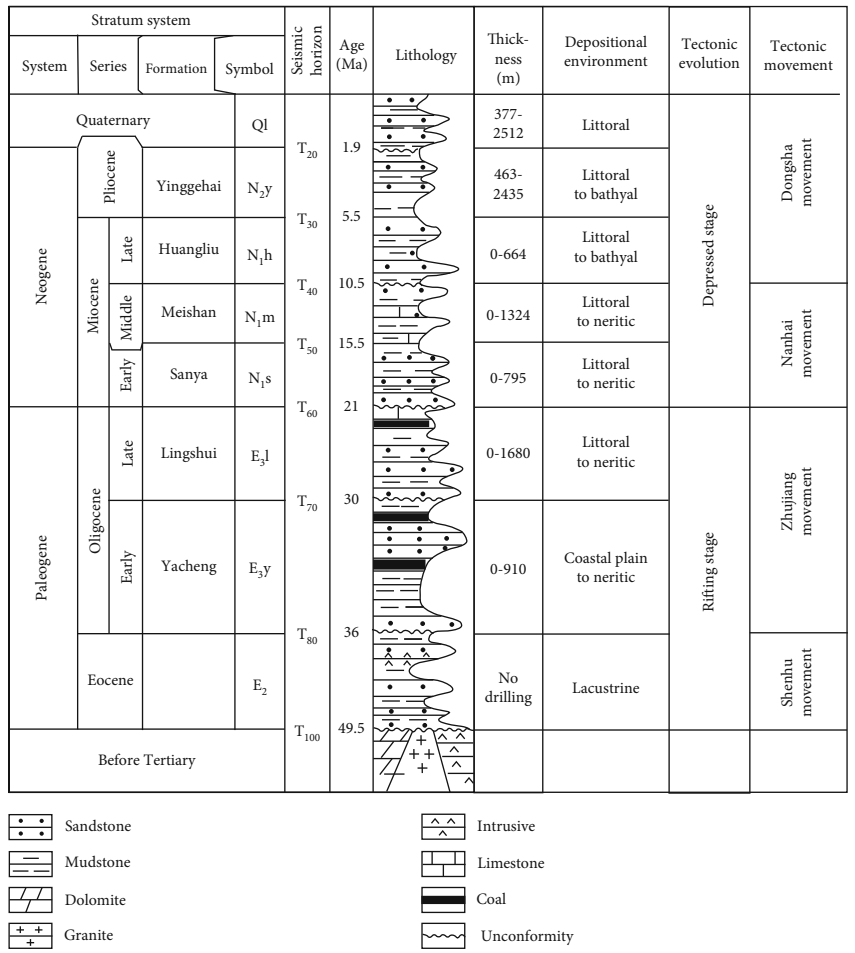

Figure 2: Stratigraphic composition and tectonic evolution in the Qiongdongnan basin.

Table 1: Diagenetic stages in the Yacheng region of the Qiongdongnan basin.

Diagenetic stage			Now geothermal temperature (°C)	Ro (%)	TAL	Tmax (°C)	Maturity	S (%)	I/S mixed layer type	Pore type	Depth (m)
Early stage	A	Early compaction and cementation	80	0.35	light-dark yellow < 2.6	405	Immature	70	Smectite	Primary pore	1600
	B	Early dissolution	115	0.5	dark-orange yellow 2.6-2.8	425	Half mature	40	Chaotic mixed		2400
Middle stage	A_1	Middle dissolution	140	0.7	dark-orange yellow 2.8-3	435	Low mature	25	Order mixed	Secondary pore	3200
	A_2		195	1.3	dark yellow-light brown 2.8-3	455	Mature	10	Superlattice order mixed		4500
	B	Late dissolution	>195	>1.3	light brown-brown > 4	>455	High mature	5			>4500

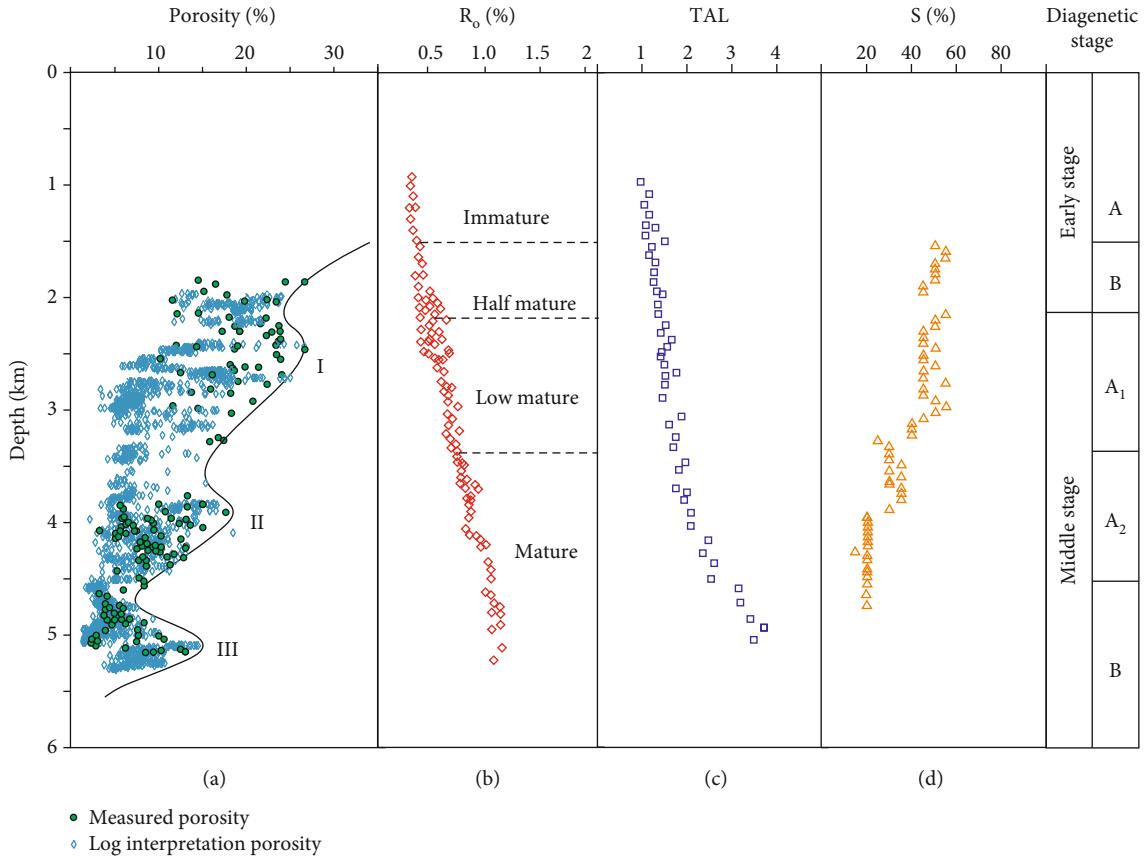

Figure 3: (a) The variation characteristics of porosity; (b) the thermal evolution of organic matter; (c) thermal alteration index from sporopollen color; (d) smectite mineral content of the illite/smectite mixed layer of the diagenetic stage in the Songtao–Baodao region of the Qiongdongnan basin. Note: Ro: organic vitrinite; TAI: thermal alteration index; S: illite/smectite mixed layer.

Q 30 m × 0.32 mm × 0.25 μm) was used, and the carrier gas was helium. The initial oven temperature was maintained at 50°C for 3 min, increased to 180°C at a rate of 15°C/min, and finally maintained for 15 min. Stable carbon isotopic values are reported in the customary ∂ notation in per mil (‰) relative to PDB (VPDB). Measurement precision was estimated to be ±0.3‰. The experiment was conducted at the Guangzhou Institute of Geochemistry, the Chinese Academy of Sciences.

Fluid inclusion analysis was carried out at the Key Laboratory of Tectonics and Petroleum Resource of Educational Ministry, China University of Geosciences. Fluid inclusion petrography was conducted using a Nikon 80I dual-channel fluorescence microscope equipped with transmitted and ultraviolet light. The main geochemical components of gas inclusions and gas-bearing inclusions were determined using a laser Raman microprobe. The homogenization temperature (Th) of fluid inclusions was measured using a LinkamTHMS600 cooling-heating stage at 20°C, i.e., room temperature. The initial heating rate was 15°C/min. The rate was set to 5°C/min when the vapor bubble in the fluid inclusion began to disappear. Measurement precision was estimated to be ±0.1°C.

4. Results

4.1. Diagenetic Stage. According to the industrial standard of the Chinese petroleum and natural gas industry (SY/T 5477-2003) [27], the diagenesis was analyzed by some parameters, such as the variation in the reflectivity of organic vitrinite (Ro), the thermal alteration index (TAI) from sporopollen color, the thermal evolution and pyrolysis parameters (Tmax), the smectite mineral content of the illite/smectite mixed layer (I/S), and the casting thin sections. The result was that the diagenetic process in the west of the Qiongdongnan basin can be divided into two stages, as shown in Table 1, the early diagenetic stage (including A and B stages) and the middle diagenetic stage (including A_1, A_2, and B stages); the corresponding depth is about 1600, 2400, 3200, 4500, and more than 4500 m (Table 1 and Figure 3).

4.2. AHPZs. AHPZ refers to the reservoir porosity exceeding that induced by the normal compaction curve with the increase in burial depth, and it is not completely equivalent to secondary porosity. The porosity variation in the Songtao–Baodao region could be obtained based on the well-logging and measured data. The plot of porosity vs. depth reveals three AHPZs at different depths (Figure 3(a)). The first AHPZ is located at 2250~3100 m with a maximum porosity close to 28%. The second and third AHPZs are located at 3700~4400 and 4800~5300 m, with porosities up to 18% and 20%, respectively. The reservoir porosity should be lower than 15% at depths below 3500 m by considering normal pore evolution regularity. This scenario suggests the

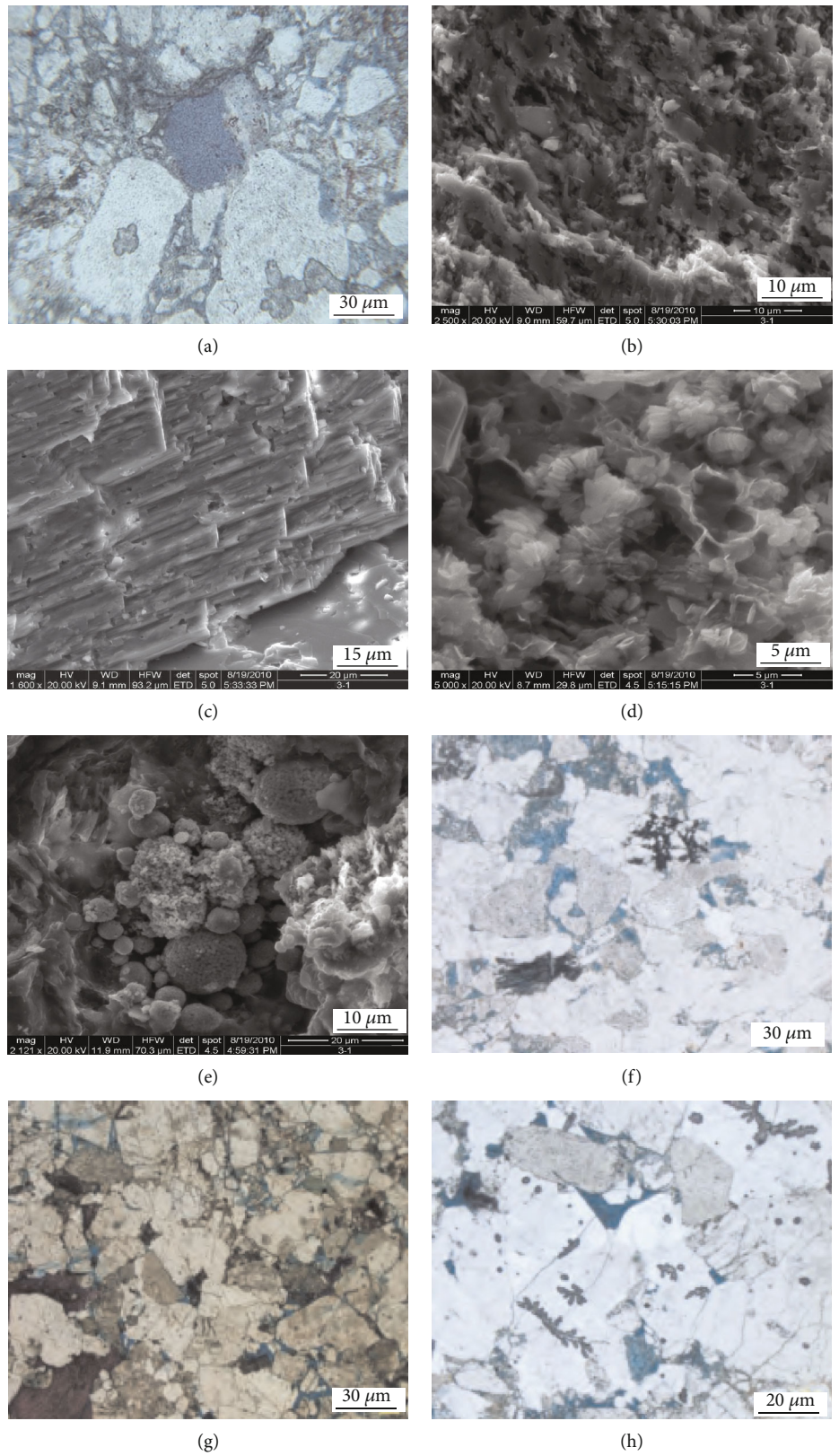

(a) (b) (c) (d) (e) (f) (g) (h)

Figure 4: Continued.

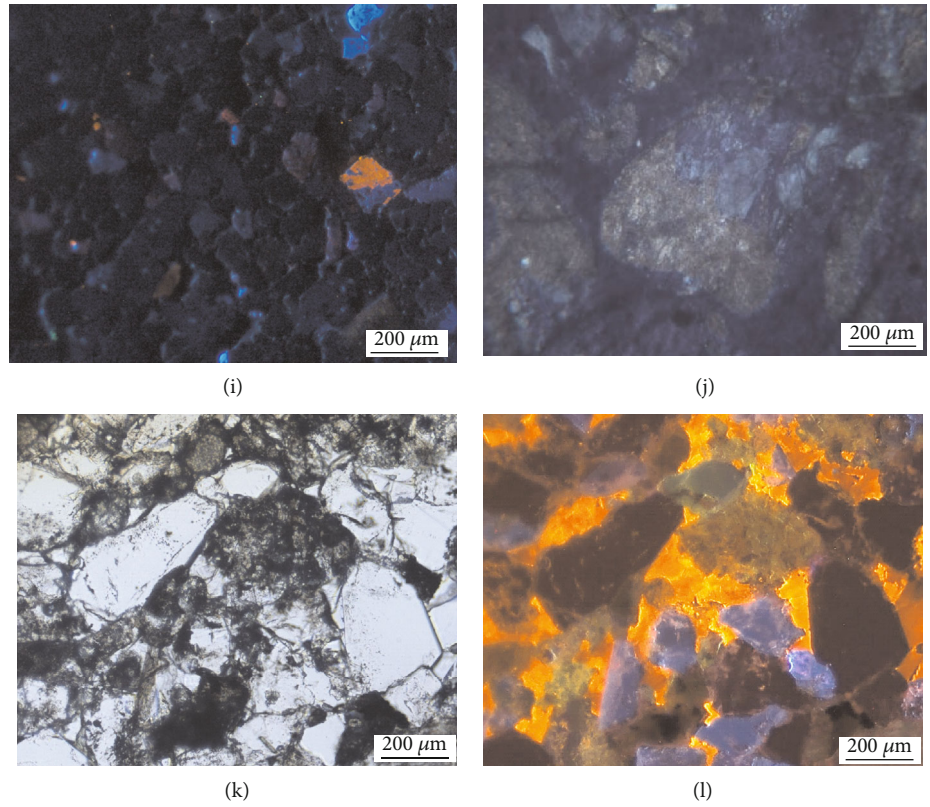

(i) (j)

(k) (l)

Figure 4: Thin section images of sandstone samples from the Songtao–Baodao region of the Qiongdongnan basin. (a) Blue cast slice; well BD15-C-A, 2268 m; feldspar dissolved into oversize molded hole. (b) Scanning electron microscopic image (SEM); well ST24-A-A, 2726 m; feldspar particles are dissolved. (c) SEM; well ST29-B-A, 2726 m; carbonate cement is dissolved. (d) SEM; well BD13-C-A, 2726 m; intergranular pores among kaolinite. (e) SEM; well ST36-A-A, 2813.2 m; berrylike pyrite. (f) Blue cast; well BD19-B-A, 4102 m; dissolved feldspar pores. (g) Blue cast; well BD19-D-A, 4102 m; dissolved feldspar pores and carbonate cement filling. (h) Blue cast; well BD19-B-B, 5092 m; dissolved feldspar and intergranular pores. (i) Cathode luminescence; well BD19-B-C, 2551.2 m; carbonate intragranular calcite cement filling the dissolved pores. (j) Orthogonal polarized light; well BD20-A-A, 2576 m; carbonate intragranular calcite cement filling the dissolved pores; well ST24-A-A, 2914.5 m. (k) Thin section; well BD19-B-B, 4100.1 m; carbonate intergranular calcite cement. (l) Cathode luminescence; well BD19-B-B, 4100.1 m; carbonate intergranular calcite cement filling the dissolved pores.

possibility of high-quality reservoirs in the middle-deep Qiongdongnan basin.

The first and second AHPZs are regional for the basin, dominated by primary pores, and followed by secondary dissolution pores. The secondary dissolution pores are mainly distributed in feldspar, rock debris, and carbonate cement, and some of them are even molded holes (Figures 4(a)–4(c), 4(g), and 4(h)). The third AHPZ is only locally developing at the Baodao 19-B structure belt and is dominated by secondary pores (Figure 4(h)). The first, second, and third AHPZs are in the middle diagenetic A1, A2, and B stages, respectively (Figure 3).

4.3. Fluid Inclusions. Fluid inclusions capture the original geofluids, which recorded the physical and chemical properties of fluid activity, such as temperature, pressure, and composition. Therefore, fluid inclusions can be used as one of the most important objects to study the geological information of paleofluid activity [28, 29]. There are three types of reservoir inclusions in the BD19-B area under microscope, including gas inclusions, oil inclusions, and CO_2 inclusions. Gas inclusions are well developed and mainly distributed in the cracks of quartz grains (Figures 5(a) and 5(b)). A large number of gas inclusions have been detected in both shallow Sanya and deep Lingshui reservoirs, which is the direct evidence of large-scale gas migration and accumulation. However, only a small amount of yellow fluorescent oil inclusion was detected in the Lingshui formation in the BD19-B structure (Figures 5(c) and 5(d)). Some three-phase CO_2 inclusions were also detected in the Lingshui reservoir (Figures 5(e) and 5(f)), indicating CO_2 filling events. Few CO_2 inclusions were found in the Sanya formation. The type of reservoir fluid observed by fluid inclusions is in good agreement with the natural gas composition of the present BD19-B structure.

5. Discussion

5.1. Reservoir Diagenetic Fluid Type and Evolution. In addition to its own properties, reservoir diagenetic fluid in the sedimentary basin is affected by external factors, including meteoric water, organic and carbonic acids, and thermal and hydrocarbon fluids [3, 4]. The property variations of diagenetic fluids in different geological periods have a large influence on the products of reaction between fluids and

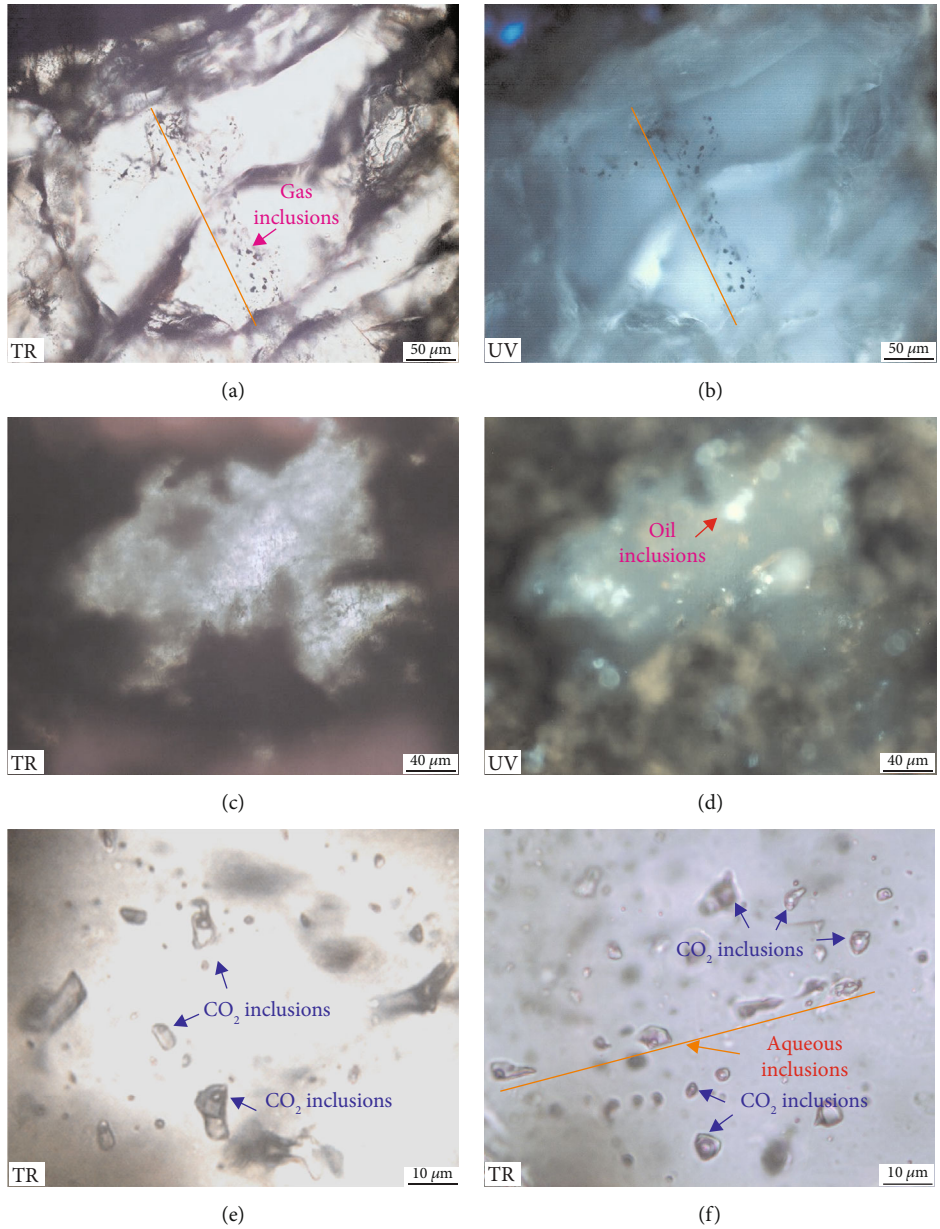

Figure 5: Fluid inclusion images of sandstone samples from the Songtao–Baodao region of the Qiongdongnan basin. TR: transmission light; UV: fluorescence. (a, b) Pure gaseous inclusions without fluorescence observed in quartz particle crack; well BD19-B-2, 3818 m. (c, d) Yellow fluorescent oil inclusions in quartz grains; well BD19-A-1, 3860 m. (e, f) Three-phase CO_2 inclusions developed in quartz particles and nearby associated aqueous inclusions; well BD19-B-1, 5155 m.

minerals in rocks. Therefore, geochemical information and mineral assemblages can be used to track the fluid types at different geological stages [30]. In this area, no obvious dissolution [25] of quartz particles suggests that minimal alkaline action was involved in the diagenetic process.

5.1.1. Organic Acid. Secondary dissolution pores in feldspar and rock debris were generally observed in three AHPZs, as well as the kaolinite and authigenic quartz near the secondary pores (Figure 4(d)), suggesting that these three AHPZs suffered from acid dissolution. Meanwhile, the relation between authigenic quartz content and depth reveals a high peak at 2250~3100 m which is in accordance with the first AHPZ (Figure 6), although the total content of authigenic quartz in the Songtao–Baodao region is low. The particles with each other show a point-line contact relationship, and no pressure dissolution or mass conversion of clay minerals at this depth range is observed (Table 1 and Figure 4). Therefore, the authigenic quartz at this depth range may form after the acid dissolution of feldspar and other minerals. These observations suggest that the dissolution was caused by organic acid. Under the action of anaerobic bacteria, organic carboxylic acid anions can be reduced to hydrogen sulfide ions, which would lead to the formation of pyrite by combining with iron ions

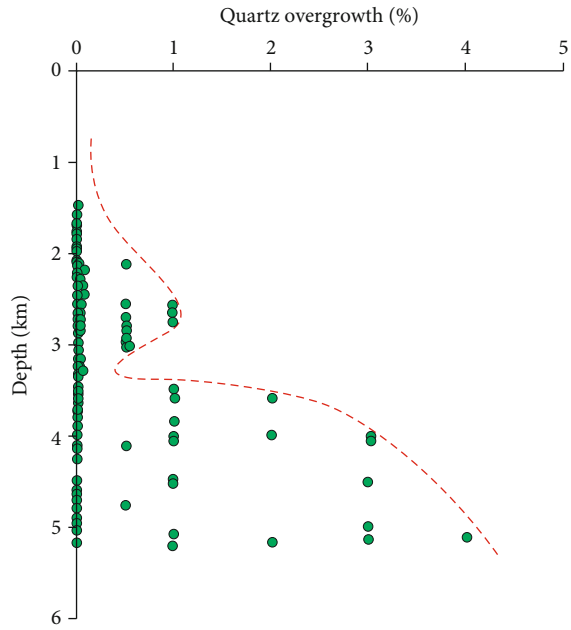

Figure 6: The variation of quartz authigenic enlargement percentage with depth in the Songtao 24-A and Baodao 19-B structure belt.

[31]. Although the content of pyrite in the first AHPZ is low, it is ubiquitous, as shown in Figure 4(e), with berrylike particles filling in pores, which also supports the involvement of organic acids.

When thermal evolution of organic matter reaches early maturity (Ro of 0.50%–0.70%), short-chain carboxylic acids will be released during kerogen degradation [32]. After the organic acid released from the source rock migrates into the reservoir, it dissolves the unstable materials, such as feldspar and rock debris, and produces secondary dissolution pores which improve reservoir quality. In the study area, the previous thermal simulation experiments show that the organic matter in the Lingshui and Yacheng Formations generated a large amount of organic acid, with an average of 3.8 mg of acid per gram of kerogen, dominated by highly soluble oxalic acid [24], which also supports the existence of organic acid in this area and the dissolution ability of the reservoir rock to dissolve.

In addition, the effective dissolution of organic acids generally occurs in the reservoir adjacent to the source rock, and the effect decreases as the distance from the reservoir to source rock increases. Using the Baodao 19-B structure belt as an example, the first AHPZ is distributed in the reservoir of the Sanya Formation, which is mainly affected by organic acid generated from the adjacent mudstone of the upper Lingshui Formation. The second AHPZ in the middle Lingshui Formation is mainly affected by the organic acids generated from its own mudstone, because the sand and mud frequently form interbeds in this formation. The third AHPZ is distributed in the reservoir of the lower Lingshui Formation, dominated by sand, and it is mainly affected by the organic acids generated from the mudstone in the middle Lingshui Formation and the coal-measure source rock of the Yacheng Formation. According to thermal evolution history, the dissolution history of organic acid can be obtained, as shown in Figure 7. Concerning this analysis, a large amount of organic acid is generated from organic matter when Ro ranges from 0.5% to 0.7%. The organic acid dissolution periods of three AHPZs are different. The first AHPZ was dissolved by organic acids roughly from the Late Miocene to the Late Pliocene. The second AHPZ was dissolved by organic acids from the Late Miocene to the Middle Pliocene. The third AHPZ was dissolved by organic acids from the Early to Middle Miocene and Late Miocene to the Middle Pliocene.

5.1.2. Meteoric Water. Large-scale meteoric water is an important factor for the development of AHPZs [33, 34]. During the basin evolution, the strata went through several tectonic uplifts and formed some unconformable surfaces [35]. At the end of the Oligocene (about 21 Ma), the Nanhai episode occurred in the basin and resulted in the strata uplift. The second AHPZ in the Lingshui Formation was uplifted to near the surface. In this geological period, the buried depth of the third AHPZ was about 1000 m and less affected by meteoric water [36, 37]. Therefore, the influence of meteoric water for the third AHPZ can be neglected. Another tectonic uplift occurred at 15.5 Ma (corresponding to the late stage of the Nanhai episode), when the first AHPZ was near the surface. The tectonic uplifts indicate that the first and second AHPZs were likely affected by meteoric water in the geologic history.

The diagenetic mineral assemblage of the water-rock reaction, such as carbonate cement, is a good tracer to track the fluid source. Carbonate cement in the study area is mainly calcite and ankerite, with a little dolomite, and the carbonate cement types are mainly intragranular calcite cement (in AHPZ I) and intergranular calcite cement (in AHPZ II) (Figures 4(j)–4(l)). The carbon isotopic value is different in different types of fluids; therefore, the carbonate cement precipitated by the fluids that provide the carbon will have different carbon isotopic values. Generally, the carbon in fluids originates from organic acid, meteoric water, and seawater. The carbon derived from the decarbonization of organic acids has a light carbon isotope with a $\delta^{13}C_{PDB}$ value as low as −8‰ to −23‰. The $\delta^{13}C_{PDB}$ provided by meteoric water generally ranges from −4‰ to −1‰. The $\delta^{13}C_{PDB}$ from seawater varies from 0 to 3‰ [38]. The oxygen isotope ($\delta^{18}O_{PDB}$) in carbonate cement is related to the formation temperature, the source of sedimentary fluid, and the diagenetic reformation in the later period [39]. Based on the types and characteristics of carbonate cement analysis, the measured carbon and oxygen isotope values of carbonate cement in the first and second AHPZs of the Baodao 19-B structure belt are shown in Table 2. The $\delta^{13}C_{PDB}$ value of the first AHPZ ranges from −3.4‰ to −0.4‰, indicating that the carbon was mainly provided by meteoric water and/or seawater. The $\delta^{13}C_{PDB}$ value of carbonate cement in the second AHPZ is lower than that of the first AHPZ, ranging from −7.9‰ to −2.2‰, suggesting that the carbon in the second AHPZ was derived from an organic carbon source.

Friedman and O'Neil suggested that oxygen isotopes in carbonate cements were determined by fractionation coefficients of the water-rock reaction, which relates to the formation

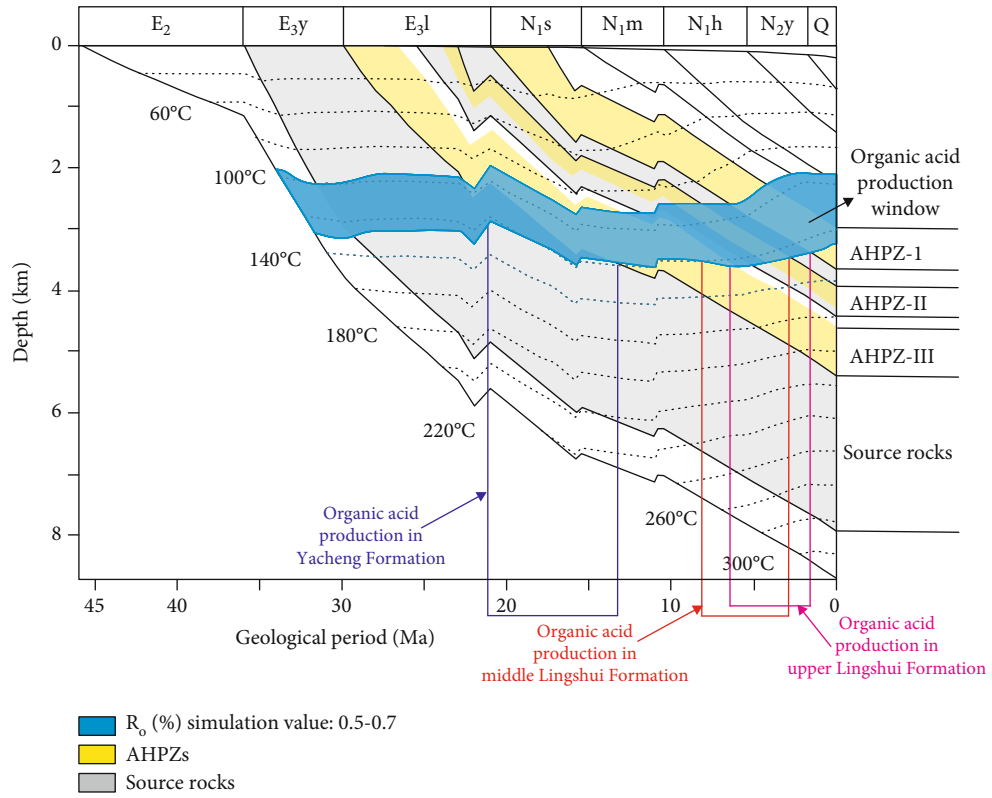

Figure 7: The burial and thermal histories of the Baodao 19-B structure belt.

Table 2: Carbon and oxygen isotopic composition of carbonate cement in the Baodao 19-B structure.

Well no.	Depth (m)	Sample location	Rock sample	Carbonate cement type	$\delta^{13}C_{PDB}$ (‰)	$\delta^{18}O_{PDB}$ (‰)
BD19-B-A	2538~2540	AHPZ-I	Borehole cuttings	Intragranular calcite cement	−2.8	−8.8
BD19-B-A	2530~2532	AHPZ-I	Borehole cuttings	Intragranular calcite cement	−2.8	−8.7
BD19-B-B	2520~2522	AHPZ-I	Borehole cuttings	Intragranular calcite cement	−2.4	−8.9
BD19-B-B	2646~2648	AHPZ-I	Borehole cuttings	Intragranular calcite cement	−0.3	−8.2
BD19-B-C	2550~2552	AHPZ-I	Borehole cuttings	Intragranular calcite cement	−3.1	−8.9
BD19-B-C	2698.0	AHPZ-I	Borehole cuttings	Intragranular calcite cement	−2.5	−9.7
BD19-B-C	2946.0	AHPZ-I	Borehole cuttings	Intragranular calcite cement	−3.4	−12.1
BD19-B-A	4189.0	AHPZ-II	Core	Intergranular calcite cement	−3.4	−10.2
BD19-B-A	4020.0	AHPZ-II	Borehole cuttings	Intergranular calcite cement	−7.9	−11.7
BD19-B-B	4100.0	AHPZ-II	Borehole cuttings	Intergranular calcite cement	−7.7	−12.2
BD19-B-B	4236.0	AHPZ-II	Core	Intergranular calcite cement	−2.2	−13.9

temperature and fluid oxygen isotopes [40]. The oxygen isotope value of the paleofluid can be deduced according to the $\delta^{13}O_{PDB}$ value and the formation temperature of carbonate cement. In this study, the formation temperatures of the first and second AHPZs were obtained from the homogenization temperature of aqueous inclusions in the dolomite (Figure 8). The formation temperature of the carbonate cement in the first AHPZ ranges from 70 to 120°C, and that of the second AHPZ ranges from 130 to 180°C. The oxygen isotope and formation temperature of the carbonate cement are plotted in Figure 9. The paleofluid oxygen isotope composition was obtained from the relationship. The oxygen isotope composition of the meteoric water is in accordance with the current rainfall value of the western Pacific [41], and the oxygen isotope composition of the seawater is the same as that of the current seawater. As shown in Figure 9, the paleofluid oxygen isotope value of the first AHPZ varies from −8‰ to +3‰. It is distributed in the mixing area of meteoric water and seawater. This phenomenon indicates that the pore fluids in the first AHPZ were mainly meteoric waters to high-salinity burial fluid in the process of

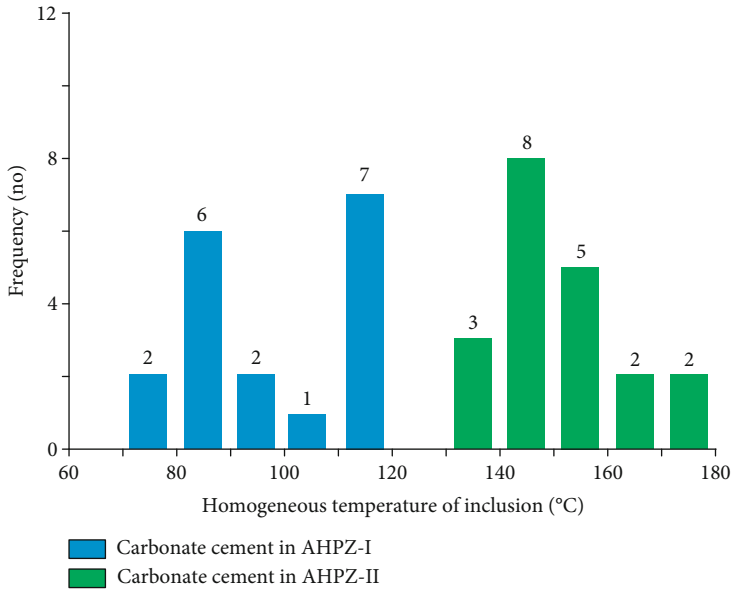

Figure 8: Homogenization temperature of the saltwater inclusion in the carbonate cement from the Songtao 29-B and Baodao 19-B structure belts.

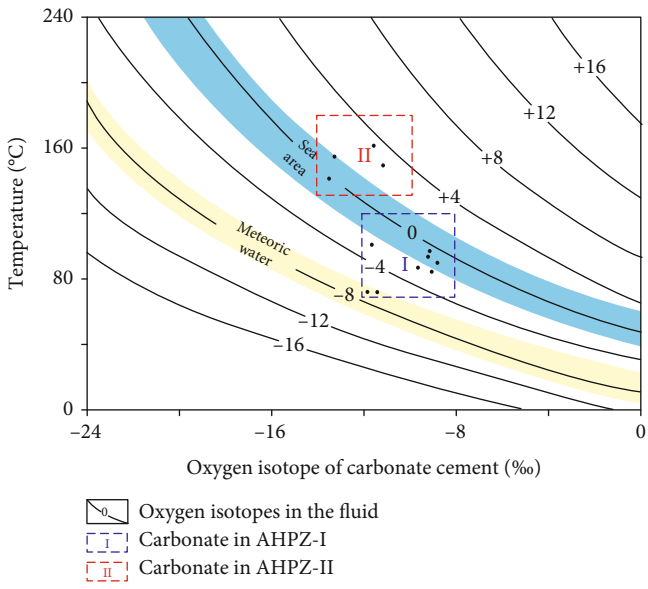

Figure 9: Diagram of the oxygen isotope and formation temperature of the carbonate cement as well as paleofluid from the Baodao 19-B structure belt.

gradual burial. The paleofluid oxygen isotope value of the second AHPZ ranges from −2‰ to +6‰, suggesting that it is seawater area with little input of meteoric water.

In addition, seawater and meteoric water could also be distinguished by salinity. The paleofluids trapped by fluid inclusions in the geological period retain the original physical and chemical properties. Therefore, the salinity of paleofluids (NaCl wt.%) can be calculated by the freezing point temperature (Tm) of the inclusions [42]. In this study, the Tm of aqueous inclusions in the first and second AHPZs were measured, and the salinity of fluids was calculated. Figure 10 shows the relationship between fluid salinity of aqueous inclusions in the first and second AHPZs. In this study, the threshold salinity of seawater and meteoric water was assumed to be 4%. The salinity of the paleofluid in the first AHPZ ranges widely from 0% to 15%, with an average value of 6.65%, indicating a mixture of seawater and meteoric water. However, the salinity of the paleofluid in the second AHPZ is relatively high, with an average value of 12.5% and a maximum of 21.5%, indicating that there was no significant input of meteoric water.

Generally, on the basis of the carbon and oxygen isotopic compositions and fluid inclusions in the carbonate cements, the origins of paleofluids in the first and second AHPZs are clarified. The paleofluids in the first and second AHPZs were mainly derived from seawater. In addition, the first AHPZ suffered from an external meteoric water at the near surface due to the tectonic uplift at the early diagenesis.

5.1.3. Thermal Fluid. Thermal fluid is a supercritical fluid and rich in a variety of minerals. It often carries high amounts of thermal energy, affecting the geothermal temperature. The Th of fluid inclusions reflects the geothermal temperature when the fluids are trapped as inclusions. Compared with the geothermal temperature, the thermal fluid activity in the basin could be determined, as shown in Figure 11. Geothermal temperatures were obtained from well drilling in the Baodao 19-B and 20-A structure belts. As shown in Figure 11, Th values of most fluid inclusions in the first AHPZ are lower than the corresponding temperatures at the same depth. However, about half of Th values in the second and third AHPZs is higher than the current testing temperature, even exceeding about 45°C. These scenarios indicate that the second and third AHPZs were affected by thermal fluids, but the first AHPZ was barely influenced by thermal fluids.

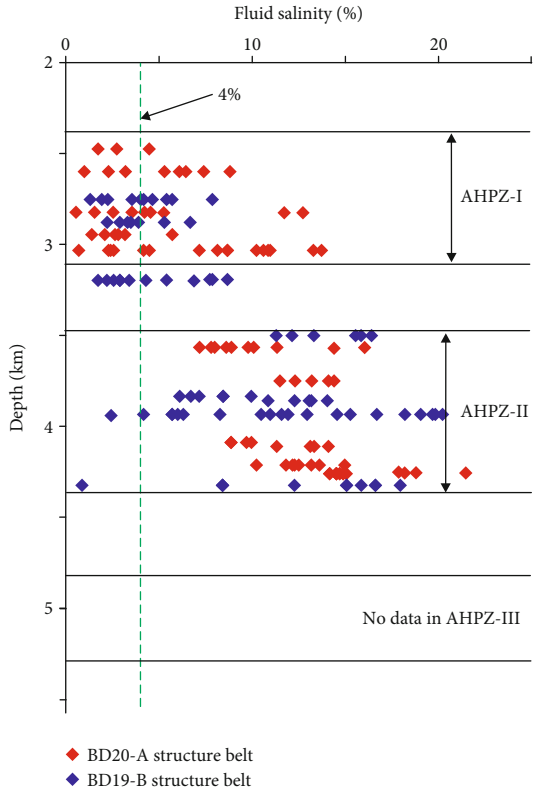

Figure 10: Relationship between fluid inclusion salinity and depth for the Baodao 20-A and 19-B structure belts.

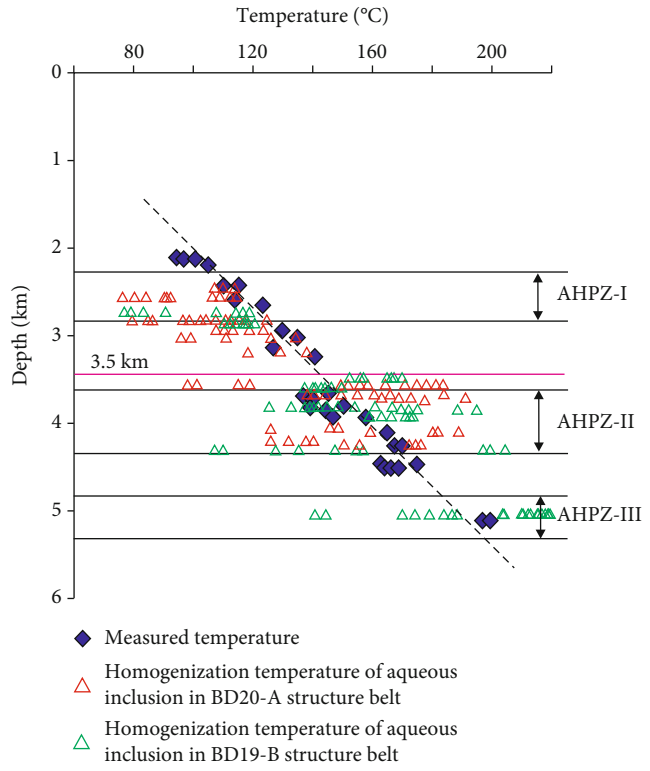

Figure 11: Relationship of the measured temperature, homogenization temperature of fluid inclusions, and buried depth in the Baodao 20-A and 19-B structure belts.

In addition, thermal fluid also greatly affects the dissolution in the reservoir due to its strong fluidity and the temperature-pressure properties. Strong fluidity can promote acid fluids to dissolve feldspar which results in more secondary pores. Meanwhile, the higher pressure and temperature can also improve the dissolution ability. This is also supported by observation of thin sections (Figures 4(f) and 4(g)). The feldspar and rock fragments were dissolved and formed dissolved pores in the second and third AHPZs, and the proportion of secondary pores to the total pores was relatively high. There is obviously high content of authigenic quartz in the second and third AHPZs, which is observably larger than in the first AHPZ (Figure 6). The abnormal overgrowth of quartz is the result of acidic dissolution. While it is impossible for organic acids to contribute so much silica, the abundant siliceous matter is likely the result of the dissolution of feldspar, rock debris, and other minerals by the active thermal fluids. Furthermore, the formation temperature of the quartz overgrowth zone may indicate the time of thermal fluids. Combining Th of inclusions in the quartz overgrowth, the active period of the thermal fluid in the Songtao–Baodao area was determined to be late stage (Figure 12).

It is noteworthy that the CO_2 content of the gas reservoirs in the third AHPZ in the Baodao 19-B belt is as high as 81.6%~87.9%. The carbon isotope value of CO_2 ranges from −7.5‰ to −6.9‰, with a $^3He/^4He$ value of 5.95×10^{-6} -8.75×10^{-6}, and an R/Ra ratio of 4.25–6.25 [26], which indicates an inorganic mantle CO_2 source [43], and may be related to the Miocene volcanic activity close to the No. 2 fault structure (Figure 1(d)). Rifting is always associated with volcanic activity, which may lead to the release of CO_2 from mantle sources. The fluid inclusion and burial history indicate that the CO_2 filling occurred in the late period (Figure 12), suggesting that the active period of thermal fluids (rich in CO_2) was also late. Under high-temperature and high-pressure conditions, the critical fluids rich in CO_2 have strong solubility to effectively dissolve feldspar and other minerals. This phenomenon is similar to that in a previous report stating that a large number of dissolution holes were discovered in high CO_2 reservoirs of the Huangliu Formation in the Dongfang gas field of the Yinggehai Basin [44, 45].

5.1.4. Hydrocarbon Fluid. The influence of hydrocarbon emplacement on diagenesis is still controversial [46]. Some scholars believe that hydrocarbon-filled pores would hinder the communication between inorganic ions and minerals [47]. Furthermore, authigenous minerals, such as quartz, illite, and carbonate cement, would be prevented from filling the pore space, and diagenesis would cease. However, other scholars have observed that hydrocarbon emplacement failed to inhibit the development of authigenic quartz and illite [48]. In this study, the fluid inclusions were used to help determine the period of hydrocarbon filling in the study area and also to analyze the effects of hydrocarbon emplacement on authigenic mineral development. The fluid inclusions in the study area may consist of gas, minor oil, and CO_2 inclusions.

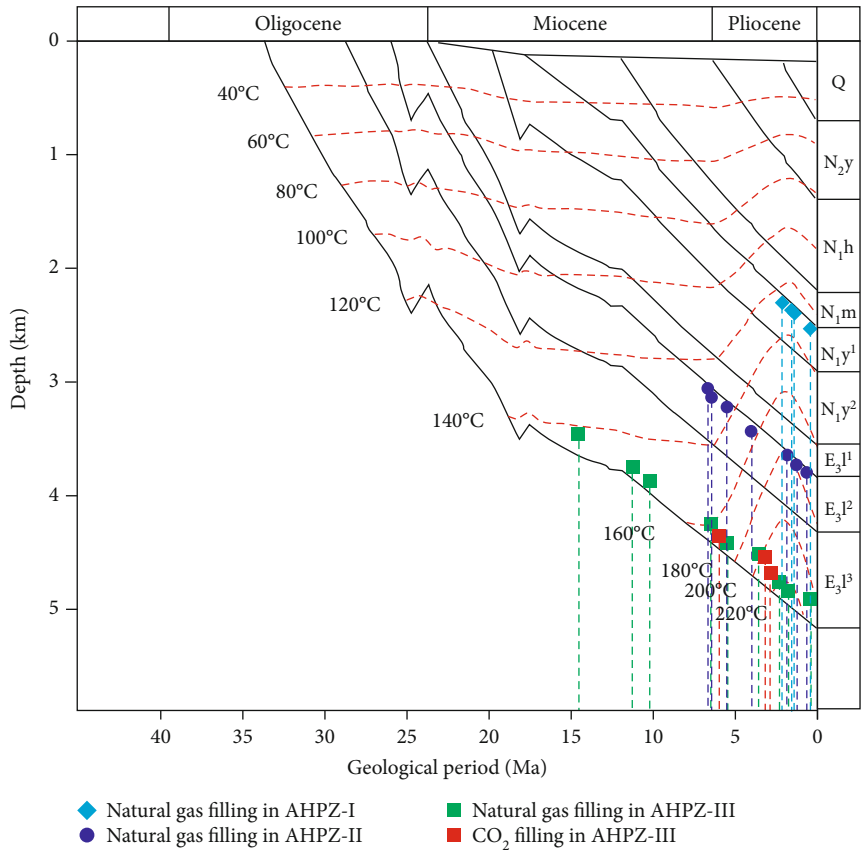

Figure 12: Natural gas filling period in the Baodao 19-A structure belt.

The inclusions present different shapes, including elliptical, triangular, and strips. The host minerals mainly include quartz grain cracks, quartz overgrowth zones, and carbonate cements (Figure 5). The development of hydrocarbon inclusions at different depths suggests that hydrocarbon migration and accumulation occurred in the geological periods. In this study, the hydrocarbons filling time in the Baodao 19-B structure belt were determined by combining the burial history and the Th of the aqueous inclusions coeval with the hydrocarbon inclusions (Figure 12). As shown in Figure 12, the time of hydrocarbon filling in the first AHPZ was after 2 Ma, in the Quaternary. The time of hydrocarbon filling in the second AHPZ was from the Early Pliocene to the present day. The time of hydrocarbon filling in the third AHPZ was from the Middle Miocene to the present day. In addition, the time of CO_2 filling was from the late Miocene to the present day. On the whole, the start time of hydrocarbon filling in the lower formation was in the early period, and that in the upper formation was in the late period, which also suggests that the lower Yacheng Formation may be the main source rock in the Songtao–Baodao structure belt.

The Th of aqueous inclusions in the quartz overgrowth and carbonate cement is similar to that of aqueous inclusions accompanying hydrocarbon inclusions, indicating that hydrocarbon filling in the study area fails to completely prevent the formation of authigenic minerals. The result may be related to gas (oil) saturation in the reservoir or more complex mechanisms. In this study, however, the carbonate cement demonstrates a certain negative correlation with gas saturation (Figure 13). The carbonate cement filling in pores is destructive to reservoir properties (Figures 4(i)–4(l)), and this negative relationship between the carbonate cement and gas saturation in the Baodao 20-A structure belt indicates that the hydrocarbon filling restrains the carbonate cement from filling of pores to a certain extent, which is favorable for reservoir porosity.

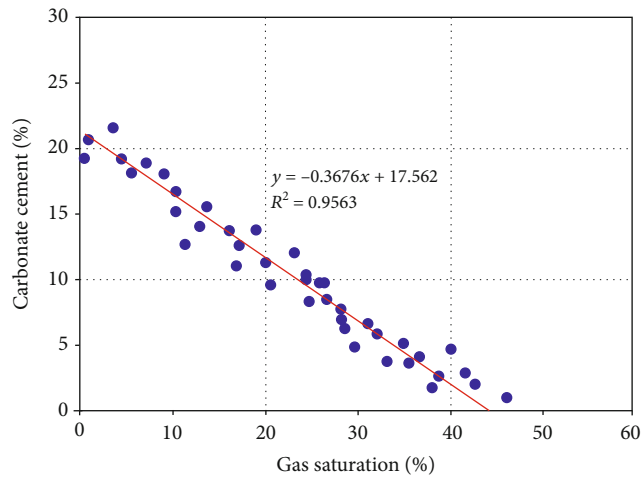

Figure 13: Relationship between the carbonate cement and gas saturation in the Songtao–Baodao region.

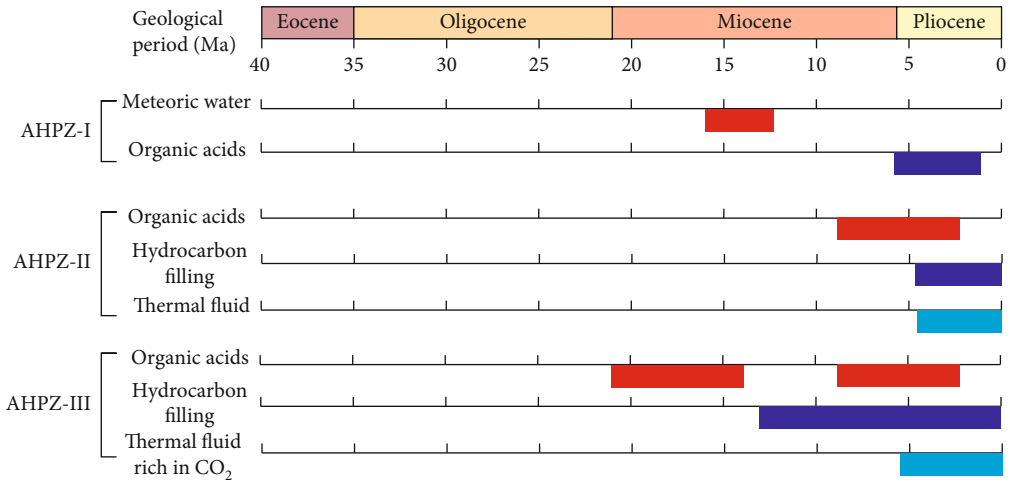

Figure 14: Diagenetic fluid types and their activity history for the Songtao–Baodao regions.

5.2. Formation Mechanism of AHPZs. The current AHPZs in the reservoir are the comprehensive results of various diagenetic fluid activities over geological periods. In this study, the diagenetic process of three AHPZs in the Songtao–Baodao region can be deduced according to the analysis of diagenetic pore fluid type and evolution (Figure 14).

Diagenetic fluids affecting the development of the first AHPZ included meteoric water, organic acid, and hydrocarbon. The meteoric water and organic acids dissolved feldspar minerals and thus led to secondary pores. The first AHPZ strata went through tectonic uplift in the Early and Middle Miocene and experienced dissolution caused by circulation of meteoric water in the shallower strata until the Middle Miocene. In the Late Miocene, plenty of organic acids were generated and expelled from the first mudstone member in the Lingshui Formation, entering the reservoir and dissolving minerals to form secondary pores. In the Quaternary, hydrocarbons began to fill the reservoir, preventing the pores from being filled and destroyed by carbonate cement to a certain extent. Finally, the first AHPZ was formed.

Organic acids, thermal fluids, and hydrocarbons were the main diagenetic fluids that led to the second AHPZ. The mechanism of organic acid dissolution and hydrocarbon filling affecting the second AHPZ is the same as that in the first AHPZ. Organic acids expelled from the second mudstone member of the Lingshui Formation in the Late Miocene caused dissolution in the second AHPZ, which was active until the Middle Pliocene. In the Early Pliocene, thermal fluid activity caused dissolution and enhanced the porosity. Meanwhile, hydrocarbon filling began to fill the reservoir, inhibiting carbonate cementation at the same time.

The third AHPZ is only found in some wells in the Baodao 19-B structure belt. The special geological location of the third AHPZ is close to the No. 2 fault where there was an active volcano and a high content of inorganic CO_2. Organic acids, thermal fluids rich in CO_2, and hydrocarbons have an important influence on the formation of AHPZ in the Baodao 19-B structure belt. In the Early Miocene, the source rock of the Yacheng Formation began to generate organic acids and caused reservoir dissolution, which was active until the Middle Miocene. In the Late Miocene, the second member mudstone of the Lingshui Formation started to generate organic acids and caused dissolution again, which was active until the Middle Pliocene. In the Middle Miocene, hydrocarbon filling inhibited the formation of carbonate cements. Meanwhile, the thermal fluid rich in mantle CO_2 began to dissolve minerals and formed secondary pores in the Pliocene, leading to the development of the third AHPZ.

6. Conclusions

The porosity variation, reservoir pore types, and corresponding diagenetic period are considered together for the identification of APHZs in the Songtao–Baodao region, eastern Qiongdongnan basin, South China Sea. There are three APHZs at depths of 2250~3100, 3700~4400, and 4800~5300 m. Moreover, the three APHZs were controlled by the multiple action of various diagenetic fluids, including meteoric water, dissolved organic acid from source rocks, thermal fluid rich in CO_2, and hydrocarbon fluids. In addition, it was concluded that three AHPZs in the Songtao–Baodao region resulted from various diagenetic fluids during different geological times.

Data Availability

Data are available on request from the corresponding author.

Conflicts of Interest

The authors declare no conflict of interest.

Authors' Contributions

X.C. and Y.W. analyzed the types and evolution of geological fluids and summarized the technical viewpoints; X.C. and A.S. analyzed the samples and organized geological data and jointly wrote the paper.

Acknowledgments

This research was funded by the Natural Science Foundation of Hubei Province, grant number 2020CFB372, and Open Foundation of Cooperative Innovation Center of Unconventional Oil and Gas (Ministry of Education & Hubei Province), grant number UOG2020-14.

References

[1] M. Hüpers, J. Ikari, B. Dugan, M. B. Underwood, and A. J. Kopf, "Origin of a zone of anomalously high porosity in the subduction inputs to Nankai Trough," *Marine Geology*, vol. 361, pp. 147–162, 2015.

[2] P. Dominic, S. Zhenbing, and S. D. Matthew, "Chemically-oscillating reactions during the diagenetic oxidation of organic matter and in the formation of granules in late Palaeoproterozoic chert from Lake Superior," *Chemical Geology*, vol. 470, pp. 33–54, 2017.

[3] G. H. Yuan, Y. C. Cao, Z. Jia, Y. Z. Wang, and T. Yang, "Research progress of abnormal high porosity zones in middle and deep clastic reservoirs in petroliferous basins," *Natural Gas Geoscience*, vol. 26, no. 1, pp. 28–42, 2016.

[4] L. Yang, L. Yu, D. Chen, K. Liu, P. Yang, and X. Li, "Effects of dolomitization on porosity during various sedimentation diagenesis processes in carbonate reservoirs," *Minerals*, vol. 10, no. 6, p. 574, 2020.

[5] P. J. Dowey, R. H. Worden, J. Utley, and D. M. Hodgson, "Sedimentary controls on modern sand grain coat formation," *Sedimentary Geology*, vol. 353, pp. 46–63, 2017.

[6] L. YOU, S. XU, C. LI, Y. ZHANG, Z. ZHAO, and P. ZHU, "Diagenesis-porosity evolution and "sweet spot" distribution of low permeability reservoirs: a case study from Oligocene Zhuhai Formation in Wenchang A sag, Pear River Mouth Basin, northern South China Sea," *Petroleum Exploration and Development*, vol. 45, no. 2, pp. 251–263, 2018.

[7] R. X. Li, S. Dong, D. Lehrmann, and L. Duan, "Tectonically driven organic fluid migration in the Dabashan Foreland Belt: evidenced by geochemistry and geothermometry of vein-filling fibrous calcite with organic inclusions," *Journal of Asian Earth Sciences*, vol. 75, no. 5, pp. 202–212, 2013.

[8] S. BARKER, S. COX, S. EGGINS, and M. GAGAN, "Microchemical evidence for episodic growth of antitaxial veins during fracture-controlled fluid flow," *Earth and Planetary Science Letters*, vol. 250, no. 1-2, pp. 331–344, 2006.

[9] S. M. Lange, S. Krause, A. C. Ritter et al., "Anaerobic microbial activity affects earliest diagenetic pathways of bivalve shells," *Sedimentology*, vol. 65, no. 4, pp. 1390–1411, 2018.

[10] U. Okyay and S. D. Khan, "Remote detection of fluid-related diagenetic mineralogical variations in the Wingate sandstone at different spatial and spectral resolutions," *International Journal of Applied Earth Observation and Geoinformation*, vol. 44, pp. 70–87, 2016.

[11] W. Patrick, H. Ulrike, K. Bastian, A. Dirk, and H. Christoph, "Critical evaluation of an upper Carboniferous tight gas sandstone reservoir: diagenesis and petrophysical aspects," *Marine and Petroleum Geology*, vol. 86, pp. 689–710, 2017.

[12] S. N. Ehrenberg, J. Zhang, and J. S. Gomes, "Regional porosity variation in Thamama-b reservoirs of Abu Dhabi," *Marine and Petroleum Geology*, vol. 114, article 104245, 2020.

[13] A. Berger, S. Gier, and P. Krois, "Porosity-preserving chlorite cements in shallow-marine volcaniclastic sandstones: evidence from Cretaceous sandstones of the Sawan gas field, Pakistan," *AAPG Bulletin*, vol. 93, no. 5, pp. 595–615, 2009.

[14] K. Violaki, J. Sciare, J. Williams, A. R. Baker, M. Martino, and N. Mihalopoulos, "Atmospheric water-soluble organic nitrogen (WSON) over marine environments: a global perspective," *Biogeosciences Discussions*, vol. 12, no. 10, pp. 3131–3140, 2015.

[15] H. Long, C. Xiang, J. Niu, and L. Wei, "Hydrothermal fluid flow and its influence on the hydrocarbon migration and accumulation along Binhai fault in Qikou sag, Bohai bay basin," *Acta Petrolei Sinica*, vol. 35, no. 4, pp. 673–684, 2014.

[16] C. C. Walters, F. C. Wang, K. Qian, C. Wu, A. S. Mennito, and Z. Wei, "Petroleum alteration by thermochemical sulfate reduction - A comprehensive molecular study of aromatic hydrocarbons and polar compounds," *Geochimica et Cosmochimica Acta*, vol. 153, pp. 37–71, 2015.

[17] J. W. Crompton, G. E. Flowers, D. Kirste, B. Hagedorn, and M. J. Sharp, "Clay mineral precipitation and low silica in glacier meltwaters explored through reaction-path modelling," *Journal of Glaciology*, vol. 61, no. 230, pp. 1061–1078, 2015.

[18] J. Peng, X. Wang, H. Han, S. Yin, Q. Xia, and B. Li, "Simulation for the dissolution mechanism of Cambrian carbonate rocks in Tarim basin, NW China," *Petroleum Exploration and Development*, vol. 45, no. 3, pp. 431–441, 2018.

[19] D. J. Smith, J. Naden, G. R. T. Jenkin, and M. Keith, "Hydrothermal alteration and fluid PH in alkaline-hosted epithermal systems," *Ore Geology Reviews*, vol. 89, pp. 772–779, 2017.

[20] Y. Chen, Y. X. Han, L. Z. Bian et al., "Geochemical characteristics and geochemical characteristics of the Paleogene sedimentary system in the northern South China Sea," *Oil & Gas Geology*, vol. 41, no. 5, pp. 1028–1037, 2020.

[21] L. Shao, A. Li, G. X. Wu, Q. Y. Li, C. L. Liu, and P. J. Qiao, "Sedimentary environment and provenance evolution of Qiongdongnan basin," *Acta Petroleum Sinica*, vol. 31, no. 4, pp. 548–552, 2010.

[22] Y. C. Zhang, X. D. Xu, J. Gan, J. T. Zhu, X. X. Guo, and X. H. He, "Geological characteristics, reservoir forming model and exploration direction of deep water gas field in Qiongdongnan basin," *Acta Geologica Sinica*, vol. 91, no. 7, pp. 1620–1633, 2017.

[23] X. M. Zeng, J. Yu, Y. Pan, X. W. Chen, and H. Zhang, "Study on the pore evolution and diagenetic facies of submarine fan in the northern slope of Lingshui sag," *Acta Sedimentologica Sinica*, vol. 36, no. 4, pp. 1198–1207, 2016.

[24] W. H. Li, Z. Z. Zhang, K. Zheng, and Y. C. Li, "geochemical characteristics and developmental models of the Eocene source rocks in the Qiongdongnan basin, northern south China sea," *Energy & Fuels*, vol. 31, no. 12, pp. 13487–13493, 2017.

[25] Y. Zhang, P. Wang, Y. Zhao, and Q. Z. Su, "Sedimentary formation and exploration significance of the Lingshui canyon system in the Qiongdongnan basin, northern South China Sea," *Journal of Oceanography*, vol. 37, no. 2, pp. 25–35, 2015.

[26] H. Su, H. Chen, X. Chen, H. P. Liu, Y. Liu, and M. Lei, "New insight into origin, accumulation and escape of natural gas in the Songdong and Baodao regions in the eastern Qiongdongnan basin, South China Sea," *Journal of Natural Gas Science and Engineering*, vol. 52, pp. 467–483, 2018.

[27] F. X. Ying, D. B. He, and Y. M. Long, *The industry standard of China and division of diagenetic stages in clastic rocks, SY/T5477-2003*, Petroleum Industry Press, Beijing, China, 2003.

[28] H. Ping, C. Li, H. Chen, S. C. George, and S. Gong, "Overpressure release: fluid inclusion evidence for a new mechanism for the formation of heavy oil," *Geology*, vol. 48, pp. 903–907, 2020.

[29] M. L. Frezzotti and S. Ferrando, "The chemical behavior of fluids released during deep subduction based on fluid inclusions," *American Mineralogist*, vol. 100, no. 2-3, pp. 352–377, 2015.

[30] J. Pszonka and M. Wendorff, "Carbonate cements and grains in submarine fan sandstones—the Cergowa beds (Oligocene, Carpathians of Poland) recorded by cathodoluminescence," *International Journal of Earth Sciences*, vol. 106, no. 1, pp. 269–282, 2017.

[31] A. Zarasvandi, Z. Fereydouni, H. Pourkaseb, M. Sadeghi, B. Mokhtari, and B. Alizadeh, "Geochemistry of trace elements and their relations with organic matter in Kuh-e-Sefid phosphorite mineralization, Zagros Mountain, Iran," *Ore Geology Reviews*, vol. 104, pp. 72–87, 2019.

[32] R. Hoffmann, D. K. Richter, R. D. Neuser et al., "Evidence for a composite organic-inorganic fabric of belemnite rostra: implications for palaeoceanography and palaeoecology," *Sedimentary Geology*, vol. 341, pp. 203–215, 2016.

[33] M. Oliveira and L. Ros, "Meteoric water and salt-dome-related diagenesis in tertiary turbidite reservoirs from the EspÍrito Santo basin, Brazil," *Journal of Sedimentary Research*, vol. 88, no. 12, pp. 1362–1380, 2018.

[34] S. W. Matthew and C. L. Kyger, "Isotopic and elemental evidence for meteoric alteration of a Pennsylvanian phylloid-algal mound holder formation, New Mexico, U.S.A," *Journal of Sedimentary Research*, vol. 85, no. 1, pp. 21–37, 2015.

[35] H. S. Shi, J. H. Yang, Y. C. Zhang, J. Gan, and J. H. Yang, "Geological knowledge innovation and a major breakthrough in deepwater natural gas exploration in Qiongdongnan Basin," *China Petroleum Exploration*, vol. 24, no. 6, pp. 691–698, 2019.

[36] J. X. Zhang, H. W. Yin, J. T. Zhu et al., "Effect of basement properties on fault structures: a case study of Qiongdongnan Basin," *Geological Journal of China Universities*, vol. 24, no. 4, pp. 563–572, 2018.

[37] B. B. Liu, X. H. Yu, J. F. Wu et al., "Half-graben types and sedimentary filling models in the continental margin basin of the northern South China Sea," *Journal of China University of Mining and Technology*, vol. 3, pp. 498–507, 2015.

[38] J. Hao, H. Liu, and P. L. Zou, "Mechanisms of natural gas accumulation and leakage in the overpressured sequences in the Yinggehai and Qiongdongnan basins, offshore South China Sea," *Earth Science Frontiers*, vol. 22, no. 1, pp. 169–180, 2015.

[39] P. Matteo, A. H. Amena, M. Daniel et al., "Impact of stylolitization on diagenesis of a lower Cretaceous carbonate reservoir from a giant oilfield, Abu Dhabi, United Arab Emirates," *Sedimentary Geology*, vol. 335, no. 15, pp. 70–92, 2016.

[40] J. Friedman and R. O'Neil, "Compilation of stable isotope fractionation factors of geochemical interest," *US Geological Survey Professional Paper*, vol. 440, no. 12, 1997.

[41] J. G. Ren, Y. P. Huang, Z. S. Fang, and X. B. Wang, "Oxygen and hydrogen isotope composition of meteoric water in the tropical West Pacific Ocean," *Acta Oceanologica Sinica*, vol. 22, pp. 60–64, 2000.

[42] K. Barbara, E. Elena, S. Jan, and H. Hanspeter, "Chemical accuracy obtained in an ab initio molecular dynamics simulation of a fluid by inclusion of a three body potential," *Chemistry*, vol. 4, no. 3, pp. 383–388, 1998.

[43] J. X. Dai, D. Z. Dong, Y. Y. Ni et al., "Some essential geological and geochemical issues about shale gas research in China," *Natural Gas Geoscience*, vol. 36, no. 6, pp. 745–760, 2020.

[44] Y. H. Xie, "Quantitative evaluation of capping ability of high temperature and high pressure cap rocks in Yinggehai basin," *Chinese Journal of Earth Sciences*, vol. 44, no. 8, pp. 2579–2589, 2019.

[45] K. Liu, Y. Sun, and Q. Q. Yu, "Characteristics of dissolutions of CO_2 geological storage applied to the Ordovician reef limestone in Bachu area of Tarim Basin," *Journal of Earth Sciences and Environment*, vol. 35, no. 3, pp. 1–4, 2013.

[46] D. Morad, F. H. Nader, M. Gasparrini et al., "Comparison of the diagenetic and reservoir quality evolution between the anticline crest and flank of an Upper Jurassic carbonate gas reservoir, Abu Dhabi, United Arab Emirates," *Sedimentary Geology*, vol. 367, no. 5, pp. 96–113, 2018.

[47] R. N. Greenberger, J. F. Mustard, E. A. Cloutis et al., "Hydrothermal alteration and diagenesis of terrestrial lacustrine pillow basalts: coordination of hyperspectral imaging with laboratory measurements," *Geochimica et Cosmochimica Acta*, vol. 175, no. 15, pp. 174–200, 2015.

[48] J. L. Soares, A. C. R. Nogueira, R. F. dos Santos, P. Sansjofre, M. Ader, and W. Truckenbrodt, "Microfacies, diagenesis and hydrocarbon potential of the Neoproterozoic cap carbonate of the southern Amazon craton," *Sedimentary Geology*, vol. 406, pp. 1–20, 2020.